Original Article

Institution of MECHANICAL ENGINEERS
Journal of PROCESS MECHANICAL ENGINEERING

Proc IMechE Part E:
J Process Mechanical Engineering
1–14

DOI: 10.1177/09544089211024065
journals.sagepub.com/home/pie
SAGE

Investigations of strain rate, size, and crack length effects on the mechanical response of polycaprolactone electrospun membranes

Ferdi C Bayram[1,*], Mehmet F Kapçı[1,*], Adile Yuruk[2], Ismail A Isoglu[2] and Burak Bal[1]

Abstract

The effects of strain rate, size (height × width), and pre-existing crack length on the mechanical response of polycaprolactone electrospun membranes were investigated by tension tests conducted at room temperature. In particular, tensile tests were performed with three different strain rates for strain rate effect tests, seven different geometries for elucidating the size effect, and three different initial notch lengths for crack growth experiments. The electrospun membranes were produced by the electrospinning technique using a polycaprolactone solution prepared in 1, 1, 1, 3, 3, 3-hexafluoro-2-propanol as the solvent. Scanning electron microscopy was utilized to show the continuous fiber structure without bead formation. The average fiber diameter was calculated as $1.113 \pm 0.270\ \mu m$ by using scanning electron microscopy images of the membranes. The chemical structure of polycaprolactone was analyzed by Fourier transform infrared spectroscopy, and the toxicity and cell viability of the electrospun membranes were shown by CellTiter 96® Aqueous One Solution Cell Proliferation Assay (MTS test). It was observed that the ultimate tensile strength and Young's modulus decreased, and the elongation at failure value increased as the strain rate decreased from 10^{-1} to $10^{-3}\ s^{-1}$. Besides, positive strain rate sensitivity was observed on the mechanical response of electrospun polycaprolactone membranes. Moreover, the dependency of mechanical response on the size geometry has been well studied, and the optimum height and width combinations were specified. Also, crack growth was studied in terms of both macroscopic and microstructural deformation mechanisms and it is observed that individual fiber deformations and interactions are highly effective on the mechanical behavior and also propagation of the crack. Consequently, in this study, the size and strain rate effects and crack growth on the mechanical response of electrospun polycaprolactone membranes have been investigated extensively, and the results presented herein constitute an essential guideline for the usage of polycaprolactone electrospun membranes at different loading scenarios.

Keywords

Mechanical characterization, crack growth, tensile tests, strain rate, electrospinning, finite-element analysis

Date received: 20 January 2021; accepted: 22 May 2021

Introduction

Electrospinning is one of the versatile techniques to produce fibers with diameters in the range of nanometers to a few microns from natural and synthetic polymers by applying electrostatic forces.[1] The basic electrospinning equipment consists of a high-voltage power supply, which transmits the charge to the polymer solution at predetermined flow rates, a digital syringe pump that forces the solution through a capillary tube, and a grounded conductive collector. The parameters of the electrospinning process, such as the solution's viscosity, applied voltage, the distance between the tip and the collector, and also environmental parameters (temperature, humidity, and airflow in the chamber) affect the fiber fabrication significantly.[2] Due to their unique properties, such as surface area to volume, interconnected pore structure, adequate mechanical strength, gas permeability, promoting cell migration and adhesion, moisture retention, and highly efficient absorption capacity, electrospun nanofibers have been applied in various biomedical fields as three-dimensional (3D) scaffolds for tissue

[1]Department of Mechanical Engineering, Abdullah Gül University, Turkey
[2]Department of Bioengineering, Abdullah Gül University, Turkey

[*]First two authors contributed equally.
Corresponding author:
Burak Bal, Department of Mechanical Engineering, Abdullah Gül University, Kayseri 38080, Turkey.
Email: burak.bal@agu.edu.tr

regeneration of bone, cartilage, tendon, dental, blood vessels, muscle, heart valves, neural tissue, and skin.[3–13]

The electrospun membranes can be fabricated from synthetic and natural polymers, and their blends.[14] Various natural polymers, such as collagen, fibrinogen, chitin, chitosan, some glycosaminoglycans, starch, dextran, alginate, and microbial polyesters (polyhydroxyalkanoates), have been widely used as electrospun membranes due to their biological characteristics, biocompatibility, similarity to macromolecules recognized by cells, and biodegradability applications.[15] Nanofibrous scaffolds prepared from natural polymers not only can mimic the native extracellular matrix (ECM) but also have structural similarities.[16,17] However, the disadvantages of the natural polymers, such as low viscoelastic properties, fast degradation rates, and limited natural resources lead the scientists to utilize the biocompatible synthetic polymers including poly(D-lactide)[18] and poly(L-lactide)[19], and their copolymers poly(D, L-lactide-co-glycolide),[20] poly-ϵ-caprolactone (PCL),[21,22] copolymers poly(L-lactide caprolactone),[23] and poly (ethylene-co-vinyl alcohol)[24] in electrospinning studies. Among the synthetic polymers, PCL has unique physical and biological properties such as biocompatibility, biodegradability with controllable degradation rate, simple and cost-effective fabrication, and adequate mechanical properties to fabricate electrospun nanofibrous membranes.[25] PCL is a Food and Drug Administration approved semi-crystalline polyester owing to its highly organized structure.[26] Besides, PCL has five hydrophobic $-CH_2$ components in its repeated units that cause slow degradation in vivo and in vitro. PCL also provides high toughness in the body since amorphous domains are in the rubbery-like structure.[27] The melting temperature of PCL is ~60 °C. Thus, electrospun membranes obtained from PCL have excellent potential for biomedical applications as biomaterials.[28,29]

Even though electrospun membranes are used in a wide variety of applications as aforementioned before, there is still a lack of information in the literature about the detailed mechanical evaluation of them. Gorrasi et al.[30] investigated the mechanical response of PCL, poly(3-hydroxybutyrate) (PHB), and the membranes based on PCL/PHB blends, which were encapsulated with curcumin at 1 wt%. In another recent study, Alexeev et al.[31] used a new method to precisely analyze the mechanical behavior of single electrospun PCL fibers. Moreover, Can-Herrera et al.[32] examined the effect of applied voltage on the morphological and mechanical properties of PCL membranes. Recent works in the literature mostly focused on the effect of processing parameters, the evaluation of mechanical behavior of pure PCL with blends, and the comparison and effectiveness of new testing methods over traditional methods. However, no current study has comprehensively examined the effects of strain rate, size, and pre-existing crack length on the mechanical properties of membranes. For that reason, the tensile test method, which is one of the simplest and the most common mechanical tests, was used in this study to determine the effects of size and strain rate on the mechanical response of electrospun PCL membranes, including ductility, ultimate tensile strength (UTS), and Young's modulus. Moreover, the effects of pre-existing cracks were investigated to understand crack propagation and microstructural deformation mechanisms. Specifically, the deformability and strength of electrospun PCL membranes are very important because they affect morphology, cell migration, and cell proliferation.[33–35] Therefore, structural integrity is substantially required for PCL membranes before new tissue formation.[15,34,36] In terms of the mechanical response of electrospun PCL membranes, research studies mostly focused on the effects of fiber diameter,[34] temperature,[37] moisture,[38] as well as the mass concentration–mechanical property relationship[39] and distribution of the fiber orientation.[40] For example, Wong et al.[41] stated that changing the fiber diameter significantly affects the tensile test results of electrospun PCL membranes. Croisier et al.[15] showed the effect of porosity percentage on the mechanical response of electrospun PCL membranes. To the best of our knowledge, a comprehensive investigation on the crack growth and effects of strain rate and size on the mechanical response of electrospun PCL membranes has never been conducted yet.

In this study, we fabricated PCL membranes using the electrospinning technique and characterized them through physical, chemical, and cell-culture studies. Afterwards, we investigated electrospun membranes using different sizes, strain rates, and pre-existing cracks' lengths to observe the change in the mechanical properties under tensile loading. In particular, the strain rate dependency of PCL membranes was studied at three different strain rates, the sensitivity to different geometrical sizes was observed by different heights and widths. Lastly, the effect of the pre-existing crack length on mechanical response as well as crack growth behavior under tensile loading was investigated by our in situ tensile test setup with a digital camera.

Materials and method

Materials

PCL (average $M_n = 80{,}000$; CAS No. 24980-41-4) was purchased from Sigma–Aldrich. 1,1,1,3,3,3-hexafluoro-2-propanol (HFIP) (CAS No.920-66-1) was purchased from Merck. Dulbecco's modified Eagle medium (DMEM), high glucose and Dulbecco's phosphate buffer saline were purchased from Biological Industries. Fetal bovine serum (FBS) and penicillin/streptomycin were purchased from Gibco. Human fibroblast cells were kindly donated by Erciyes University Genom and Stem Cell Center, Kayseri. All other reagents were of analytical grade and used as received.

Preparation of electrospun membranes

In our previous studies,[13] we mainly used the electrospinning technique and prepared electrospun PCL membranes. Thus, the electrospinning parameters including

the flow rate, the voltage, and the distance between the tip and the collector were finely optimized to obtain a bead-free and uniform fiber structure without any defects, which were also utilized in this study. Briefly, PCL pellets were dissolved at a concentration of 10% (w/v) in HFIP and stirred for 8 h at room temperature to obtain a homogeneous polymer solution. Afterwards, the polymer solution was taken in a syringe having a 21 G needle, which has an inner diameter of 14.53 mm. The syringe was oriented to a motorized and programmable syringe pump (NE-1000 syringe pump) to set the flow rate of the polymer solution as 0.8 ml/h. The grounded collector covered with an aluminum sheet was positioned opposite to the tip of the syringe at a distance of 15 cm. A voltage of 15 kV was applied by a high-voltage power supply (NE100, Inovenso, Turkey). The fluid jet was ejected from the tip of the syringe. As the jet accelerated toward the grounded collector, the solvent evaporated, and the polymer nanofibers were deposited on the collector in the form of a nonwoven fabric, that is, the electrospun PCL membrane.

Morphological analysis

A scanning electron microscope (SEM, ZEISS LS-10, ERNAM, Erciyes University) was used to investigate the fiber morphology of the membranes. After being vacuum coated with a thin layer of gold (QUORUM, Q150R ES), the fibers were scanned by using the SEM at 25 kV. The diameters of the nanofibers were calculated from the SEM image by using Image J software. In addition, x-ray diffraction (XRD) was carried out to observe the diffraction peaks and degree of crystallinity.

Cytotoxicity test

The viability of the human fibroblast cells on the PCL electrospun membranes was determined by using the MTS assay (CellTiter 96®, Promega, Madison, WI, USA). Briefly, membranes were located in the 96-well plates. All these membranes represented a 3D system and were compared with two-dimensional (2D) as control. The PCL electrospun membranes were first sterilized by treating them with 70% ethanol and saturated with DMEM media (DMEM high glucose) containing 10% FBS and 1% penicillin/streptomycin at 37 °C for 24, 48, and 72 h. The human fibroblasts were seeded onto the PCL membranes at a seeding density of 1×10^5 cells/ml, whereas control wells had only cells supplemented with a complete medium without membranes. Cell seeded membranes were incubated at 37 °C in an incubator with humidified 5% CO_2. Pipet 10 µl of CellTiter 96® AQueous One Solution Reagent into each well of the 96-well assay plate containing the samples in 100 µl of culture medium, the plate was incubated at 37 °C for 2 h in a humidified, 5% CO_2 atmosphere. Record the absorbance at 490 nm using a 96-well plate reader (Varioscan Lux, Thermo Scientific).

Chemical analysis

Infrared spectroscopic analysis was conducted to characterize functional groups in the PCL to confirm the presence of the membrane component phases and to discern any possible chemical modification or interaction between phases. A Fourier transform infrared spectroscopy (FTIR) spectrum of the PCL membrane was recorded on a Nicolet 6700 spectrometer (Nicolet 6700, Thermo Scientific).

Mechanical testing

Strain rate effect tests. To understand the strain rate sensitivity of the electrospun membranes, they were subjected to tensile tests at three different strain rates of 1×10^{-1}, 1×10^{-2}, and 1×10^{-3} s^{-1}, respectively. Quasi-static strain rates have been selected during the tensile tests because these polymeric membranes are subjected to similar strain rates in service environments. The predetermined sample dimensions used in tensile testing were 70 mm in length with 20 mm gauge length, 20 mm in width, and 0.2 ± 0.02 mm thickness. All specimens used for tensile testing were cut into the same dimensions precisely to prevent any possible size effect on the mechanical response of electrospun PCL membranes. The tensile tests were performed three times at each strain rate to ensure the consistency of the results.

Size effect tests. Once the electrospun membranes were fabricated and prepared by the electrospinning process, the electrospun membranes were cut into different geometries with different width and height dimensions. The length of the prepared electrospun PCL membranes was 70 mm with different gauge height and width dimensions. The PCL specimens were cut into various width sizes carefully and optical microscopy was performed to ensure the precision of the cutting operation. A quasi-static initial strain rate, 1×10^{-3} s^{-1}, was utilized to study the effect of size on the mechanical behavior. The specimens were mounted on the tensile test grips and then all the tests were conducted until the specimens were ruptured. All tensile tests were repeated three times to ensure the consistency of the obtained results. All tensile tests were carried out using a servo-hydraulic universal tensile testing machine Shimadzu AGS-X with a load capacity of 10 kN.

Crack propagation tests. Crack propagation tests of the electrospun membranes were conducted again on 20 mm × 20 mm gauge size specimens with initial notch lengths of 1, 3, and 5 mm that are placed at the center of one edge of the membrane perpendicular to the loading direction. To understand the 2D strain formations during the deformation, the digital image correlation (DIC) technique was utilized with Open-Source MATLAB-based image processing software Ncorr. For image tracing, a random speckle pattern was formed on the white specimen surface by spraying a black paint

solution. The region of interest was adjusted as a whole gauge and one image was extracted for each second from the video recorded during deformation. All specimens were subjected to 0.2 mm/s crosshead displacement speed until total rupture occurs. After these tests, specimens with 3 mm pre-existing crack size deformed up to critical points and the region ahead of the crack tip evaluated by SEM to observe microstructural deformation mechanisms. Specifically, uniaxial tension is applied to the specimens where the deformation reaches the elastic region prior to the yielding and plastic regions after yielding, prior to necking and after necking.

Finite-element analysis

Finite-element (FE) analysis of the specimens with pre-existing cracks was conducted by commercial ABAQUS software to observe hydrostatic stress distribution with regard to distance to crack tip. The initial geometry for each notch length model was constructed as 20×20 mm ($W \times L$) for x and y directions, respectively, with 0.2 mm thickness along the z direction. Subsequently, 1, 3, and 5 mm notches were formed at the middle of one side of the membrane such that the crack plane normal is along the loading direction y. Thereafter, boundary conditions were set as fixing the bottom plane of the membrane normal to the y-direction and applying displacement on to the upper plane along the y-direction with a uniform 0.2 mm/s crosshead displacement speed. The linear hexahedral mesh was defined along the whole geometry with extremely fine meshes near the crack tip. To define material response, experimental stress–strain response of the unnotched sample was introduced into the FE model and the ductile damage model was used by a fracture strain parameter. Lagrangian strain data obtained by the DIC method were used for the calculation of the equivalent von mises fracture strain. The calculation was conducted on strains ahead of the crack tip before the step that crack propagation initiates through a membrane. Simulations for all notched samples were conducted until the step before yielding occurs. For comparison of hydrostatic stress distribution, pressure values were obtained ahead of the crack tip in the direction parallel to the crack plane normal.

Results and discussion

Morphological characterization

The PCL electrospun membranes were characterized morphologically by using SEM, as shown in Figure 1. As optimum electrospinning conditions, the voltage applied was set to 12.5 kV; the flow rate was set to 0.8 ml/h, and the distance between the tip and collector was set to 15 cm to obtain electrospun membranes possessing a bead-free fiber structure. The SEM results show the uniform structure of the fibers without any defects. These fibers are smooth, bead-free, highly continuous, and in a cylindrical shape with a mean diameter of 1.113 ± 0.270 µm.

In the literature, Drilling et al. [42] fabricated electrospun membranes with an average diameter of 900 ± 60 nm from the PCL dissolved in acetone (18%, w/v). Besides, they also investigated electrospun membranes with an average diameter of 790 nm, which was obtained from the PCL solution (6.7%, w/v) prepared using HFIP. In another study, Drexler et al.[43] prepared electrospun membranes from an 8% PCL/HFIP solution with a fiber diameter of 1.100 ± 0.200 µm. According to the literature, it was concluded that the mean diameter of PCL electrospun fibers given herein is consistent with previous studies.

Chemical characterization

The chemical structure of the PCL electrospun membrane was analyzed by FTIR. The characteristic PCL polymer absorption peaks at 2943 and 2865 cm^{-1} correspond to the asymmetric $–CH_2$ stretching and symmetric $–CH_2$ stretching, respectively.[44] According to Oliveira et al. PCL shows strong bands as a carbonyl stretching mode, $\sim$1726 cm^{-1}.[45] Also, the PCL has asymmetric COC stretching at 1238 cm^{-1}.

Furthermore, the peaks observed at 1470, 1417, 1396, and 1364 cm^{-1} are due to $–CH_2$ bending vibrations. The crystalline PCL is appointed to the backbone C–C and

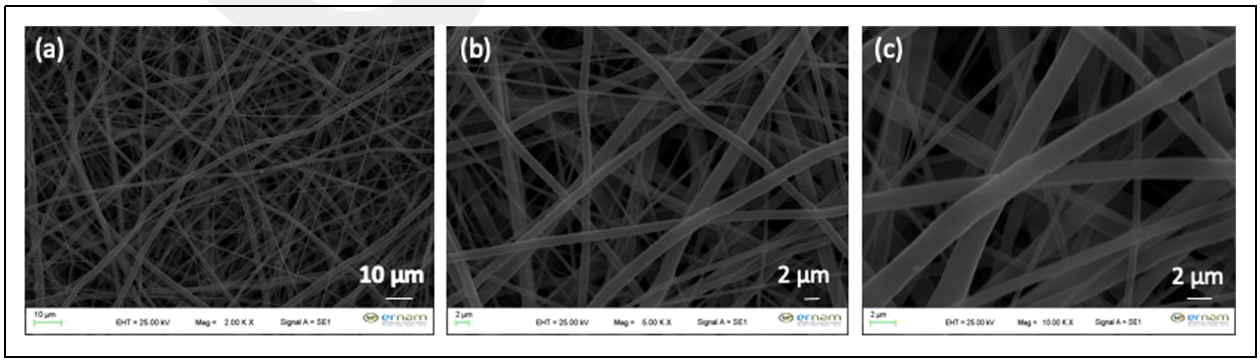

Figure 1. SEM images of an electrospun PCL membrane taken prior to tensile tests. (a) 2000× magnification, (b) 5000× magnification, and (c) 10,000× magnification.
SEM: scanning electron microscopy; PCL: polycaprolactone.

C–O stretching around 1294 cm^{-1}.[46] He et al. reported that the numerical investigation of PCL crystallinity at the carbonyl vibration region, which includes amorphous and crystalline bands at 1736 cm^{-1}.[47] The FTIR spectrum successfully indicated all characteristic peaks of PCL.[44]

Cell viability of electrospun membranes

MTS assay was conducted to evaluate the biocompatibility of electrospun membranes and show the viability (%) of human fibroblast cells on electrospun membranes following 24, 48, and 72h of culture. According to the results, the electrospun membrane showed no significant differences in cytotoxicity at the predetermined time of culture. Cell viability was calculated to be >87% for all membranes, which approves that the membranes have no cytotoxic effects. Data points are the average of $n = 6$.

Biocompatibility is one of the essential features of the electrospun membranes, which is a result of the complex interactions between the material and the surrounding tissue. The adequate surface chemistry, fiber orientation, and specific functional groups of the material affect biocompatibility and have an active role in cell adhesion, proliferation, and attachment.[48] Based on these facts, PCL with O–(CH_2–)5–CO– units in its chemical structure provides excellent biodegradability and biocompatibility.[27] Besides, some studies revealed that the fiber morphology and surface topography of the electrospun membranes prepared from PCL enhance the cell attachment and spreading due to their morphological similarity with the native ECM. Thus, our results confirmed that PCL electrospun membranes prepared in this study are favorable and biocompatible for attachment and migration of human fibroblasts on the membranes.

XRD result of PCL membranes

X-ray diffraction (XRD) analysis of the PCL membranes was conducted by using a Bruker D8 Discover X-ray diffractometer operating at 40 kV and 40 mA with a Cu-Kα source. Bragg angles $2\theta = 21.3°$ and 23.6° were identified as strong diffraction peaks, which correspond to (110) and (200) reflections, respectively.[48,49] Moreover, the XRD analysis also provided information about the degree of crystallinity as 45.9%, which is well consistent with the previous studies reported in the literature.[50,51]

Mechanical behavior

Strain rate effect. The engineering stress–engineering strain responses of electrospun PCL membranes and the corresponding tensile properties at different strain rates are given in Figure 2 and Supplemental Table 1, respectively. All electrospun membranes showed a linear elastic response together with distinct yield stress and significant

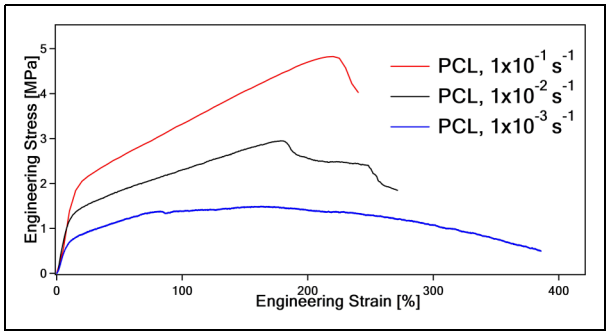

Figure 2. The engineering stress–strain curves of electrospun polycaprolactone (PCL) membranes at different strain rates.

plasticity, and a similar mechanical behavior was well observed previously in semi-crystalline polymeric materials under tensile loading.[15,36,41] PCL electrospun membranes showed a positive strain rate sensitivity, meaning that yield strength values remarkably increased at higher strain rates. In other words, yield stress and tensile stress values have prominently increased as a consequence of pulling the membranes at a faster rate. This increase of both stresses is associated with the secondary relaxation process that is the increase in the rate of loadings will reduce the polymer chains' molecular mobility and thus results in stiffer chains. Thus, these stiffer polymer chains make PCL membranes harder and failure occurs at the early stages compared to lower strain rates. In particular, the UTS of the PCL membrane increased from 1.39 to 3.16 MPa and then to 4.80 MPa when the strain rate was increased from 1×10^{-3} to 1×10^{-2} s^{-1} and further increase to 1×10^{-1} s^{-1}. However, the ductility of the PCL membrane decreased with increasing strain rate. The increase in the ductility at lower strain rates could be attributed to the fact that electrospun PCL fibers find enough time to elongate which results in thinner fibers. The average fiber diameter was found to be about 0.5 μm at a 1×10^{-3} s^{-1} strain rate and is approximately twice thinner than the test performed at a 1×10^{-1} s^{-1} strain rate as shown in Figure 3(d). A similar behavior was also observed previously in different polymeric materials[52,53] as well as other material types such as metals and ceramics.[54–56]

It is well known that the mechanical response of polymers as other materials groups, metals, and composites, depends on the strain rate either positively or negatively.[57–59] Positive strain rate sensitivity is attributed to the fact that when the material is deformed at a faster rate, the plastic deformation mechanisms and their interactions with each other are enhanced and increase the stress level.[60,61] Therefore, understanding the fundamental deformation mechanisms of the PCL membranes by observing the microstructure at different strain rates is of utmost importance to discuss the observed strain rate sensitivity (Figure 2). Since electrospun PCL membranes possess hyperplastic behavior during the deformation process, strain rate dependence significantly affects the mechanical properties.

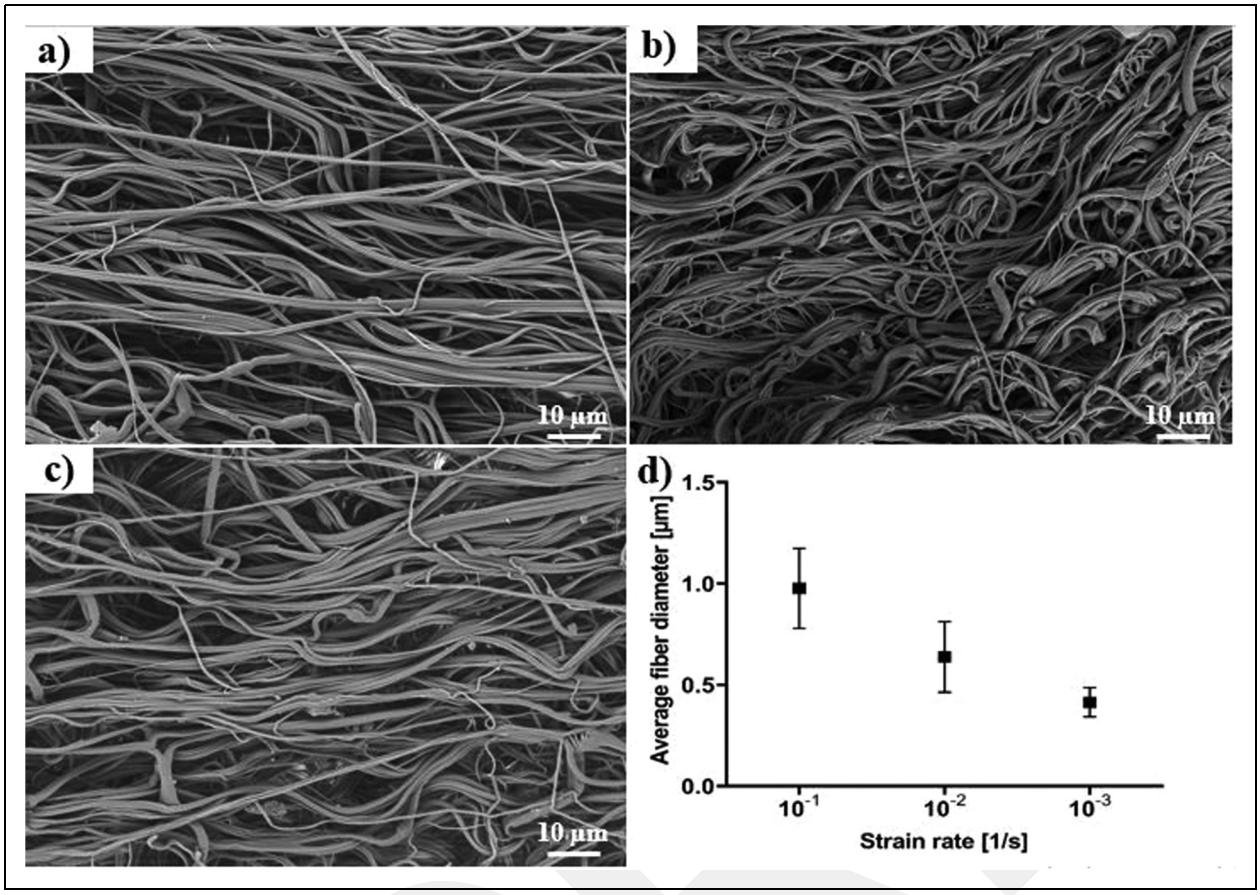

Figure 3. SEM of electrospun PCL membranes at different strain rates (a) 10^{-1} s^{-1}, (b) 10^{-2} s^{-1}, (c) 10^{-3} s^{-1}, and (d) average fiber diameters at each strain rate.
SEM: scanning electron microscopy; PCL: polycaprolactone.

Figure 3 shows the SEM images of the electrospun PCL membranes conducted at different strain rates, and their corresponding average fiber diameters subsequent to a total rupture are given in Figure 3(d). To obtain the average fiber diameter, nine different fibers from each SEM figure (Figure 3(a) to (c)) were randomly selected and measured by using ImageJ software (National Institutes of Health, Bethesda, MD). Figure 3(d) clearly shows that the average fiber diameter was decreased as the strain rate decreased from 10^{-1} to 10^{-3} s^{-1}. The decrease in average fiber diameter as the strain rate decreases can be attributed to the fact that the fibers could find enough time for the elongation at a relatively low strain rate, 10^{-3} s^{-1}, whereas, at higher strain rates, fibers could not find enough time for stretching and elongation and a sudden premature fracture occurred. As can be seen in Figure 2 that the PCL membrane with the slowest strain rate was elongated nearly two times more than the PCL membrane with the fastest strain rate. Thus, the more the PCL membrane elongates, the thinner the fiber diameters become (Figure 3(d)). The average duration of tensile tests was 1, 5, and 35 min for 10^{-1}, 10^{-2}, and 10^{-3} s^{-1}, respectively. In addition, the thinner fiber the PCL membrane has, the less strength and the more ductility it exhibits.

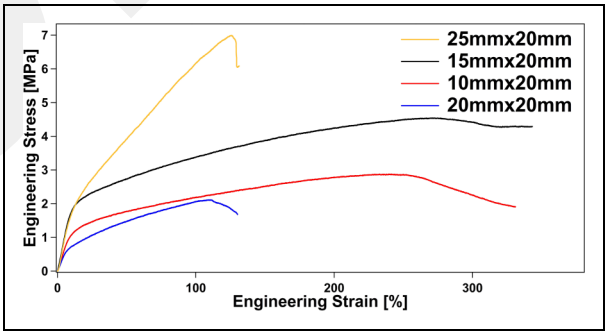

Figure 4. The engineering tensile stress–strain curves of electrospun polycaprolactone (PCL) membranes with the same width and different height dimensions for size effect comparison.

These observations were reported previously, and our conclusion agrees well with them.[62,63]

Size effect. Figure 4 shows the specimen length dependency of the mechanical response of the electrospun PCL membranes conducted at a strain rate of 10^{-3} s^{-1}. The PCL membranes with 10 and 15 mm lengths exhibited the highest ductility values around 350% elongation and

possessed moderate strength values with 2.86 and 4.53 MPa, respectively. As the length of the specimens increased from 15 to 20 and 25 mm, the decrease in ductility was more than twice but tensile strength has remarkably increased. The PCL membrane with 20 mm in height possessed the highest tensile strength (7.16 MPa) and Young's modulus (17.27 MPa) values but possessed lower ductility values when compared to shorter length specimens. A line of best fit was drawn for the elastic region and the slope of the line gave us Young's modulus of membranes. Briefly stated, while longer length PCL membrane specimens (20 and 25 mm in length) exhibited similar mechanical properties with high strength and moderate ductility values, shorter length PCL membranes (10 and 15 mm in length), on the other hand, possessed identical mechanical behavior with high ductility and moderate strength values. It is obvious that the mechanical behavior of PCL membranes depends on the size of the sample as well as the strain rate. Overall, the total percentage of elongation decreases and tensile strength increases with an increase in length of the specimens. In particular, the PCL membrane with 15 mm height exhibited the best ductility and strength combinations under tensile loading with the values of 4.53 MPa and 343%, respectively. On the other hand, the PCL membrane with 10 mm height exhibited the lowest Young's modulus of 6.46 MPa and the UTS of 2.31 MPa. Thus, the PCL membranes with longer lengths (20 and 25 mm heights) could be preferred in the applications such as cartilage repair where high strength is of first priority than the ductility phenomenon.[64] On the other hand, the PCL membranes with shorter gauge lengths could be a better choice for the applications such as wound dressings and skin tissue engineering applications where total elongation is of utmost importance than tensile strength since elongation at break of native human skin is 35% to 115%, which matches the mechanical properties of the PCL membranes with 10 and 15 mm heights.[65]

Figure 5 shows the engineering stress–strain curves for the width size dependence of electrospun PCL membranes with changing width size from 10 to 15, 20, and 25 mm with the same height of 20 mm. The smallest width-sized PCL membrane with 10 mm exhibited the highest total percent elongation up to 277%. However, the ductility trend showed a falling tendency as the width length of PCL membranes increased from 10 to 15 and 20 mm. Moreover, tensile strength and Young's modulus characteristics gradually enhanced, unlike the total elongation behavior. The PCL membrane with 25 mm width length possessed higher ductility but lower strength than the one with 20 mm width size. Thus, increasing the width size will not always improve the combination of strength and ductility properties together. Therefore, the size effect of PCL membranes at different rates of loadings should be taken into consideration in the area of usages. Similar to height–size dependence, the PCL membrane with 20 mm could be used in applications that high strength is desired. Additionally, shorter width sizes could be used when ductility is the priority in the field of usages. It is clear that changing the specimen geometries altered the mechanical response of electrospun PCL membranes, as clearly shown in Figures 4 and 5.

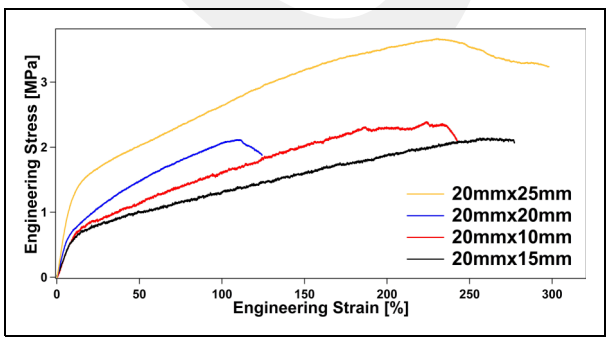

Figure 5. The engineering tensile stress–strain curves of electrospun polycaprolactone (PCL) membranes with the same height and different width dimensions for size effect comparison.

Figure 6 shows the 3D response surfaces of elongation, UTS, and Young's modulus as a function of height and width dimensions. A 10 mm height provided high elongation, as clearly shown in Figure 6(a) with red regions. However, when the height increased to 20 mm, a sudden decrease occurred in elongation, which is illustrated with a blue region. The 3D response surface plot clearly showed that the total elongation exhibited a decreasing tendency as the height of the PCL membranes increased. In particular, 20 mm height is the critical value for all membranes since all the mechanical properties were prominently degraded at this value. In addition, membranes possessing 25 mm in height and 20 mm in width provided the optimum combination of strength and Young's modulus. Moreover, no direct correlation was observed between the mechanical properties and the order of specimen sizes. According to the previous studies for metallic materials in the literature, the yield strength and UTS did not get affected significantly by changing specimen size; however, elongation at break values changed by each geometry size.[44,57] However, in this study, it has been demonstrated that specimen geometry has a significant effect on the mechanical response of the electrospun PCL membrane.

Crack propagation and finite-element analysis. Stress and displacement response of unnotched and notched specimens with initial lengths of 1, 3, and 5 mm are shown in Figure 7. It is observed that each specimen exhibits a ductile failure. However, the initial notch size highly affects the UTS as well as the ductility of the PCL membrane. Such an initial notch size dependence on the failure displacement and strength is also observed in previous studies on electrospun nanofiber containing microstructures.[66] Each specimen independent of the initial notch length

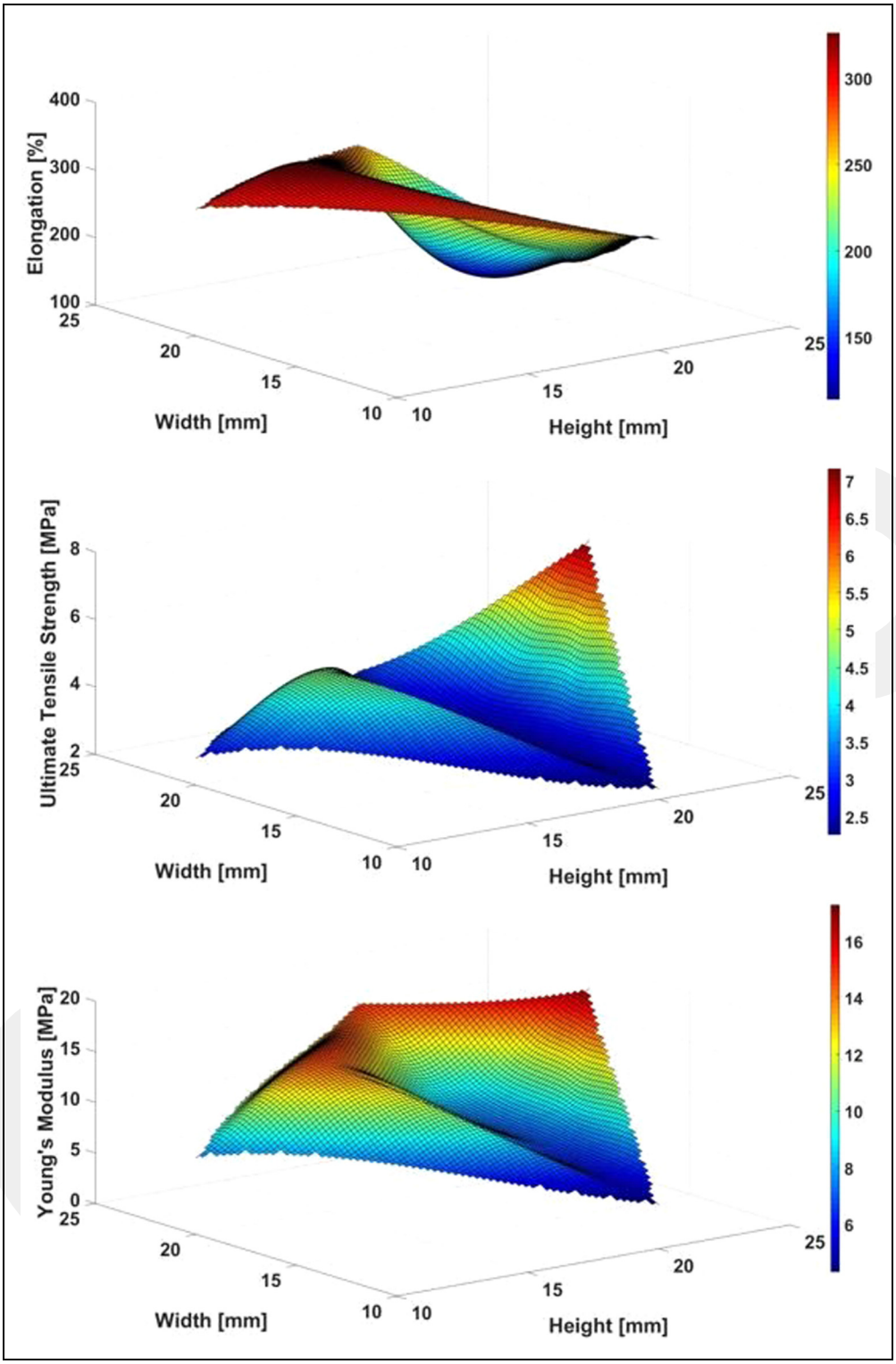

Figure 6. Response surface plots (3D) showing the effects of different height and width sizes on elongation, UTS, and Young's modulus.
3D: three dimensional; UTS: ultimate tensile strength.

reveals approximately similar strain hardening modulus and Young's modulus. Reduction in the thickness of the specimen set used in the crack propagation tests caused an overall engineering stress increase compared to strain rate effect tests.

For each notched specimen, increasing stress concentration around the crack tip induces blunting of the crack until plastic region before necking so that crack length remains constant while crack tip opening displacement increases. After the local strain reaches

a critical point, cleavage starts through the membrane, whereas blunting is still active till the necking point. However, as engineering stress reaches the necking point, the propagation of the crack rapidly increases and total rupture occurs eventually. Depending upon the accumulated local strain around the crack tip, cleavage starts at earlier displacement for higher initial notch lengths. Figure 8 obtained from the DIC for a 5 mm notched specimen reveals arising *y*-direction Eulerian–Almansi strains around the crack tip at various displacement levels. It can be observed that until the necking point crack blunting mechanism proceeds, whereas there is a slight crack tip advance by cleavage. However, by an increase of the total displacement, strain accumulates ahead of the crack tip gradually which leads to a local tear and initiation of the cleavage.

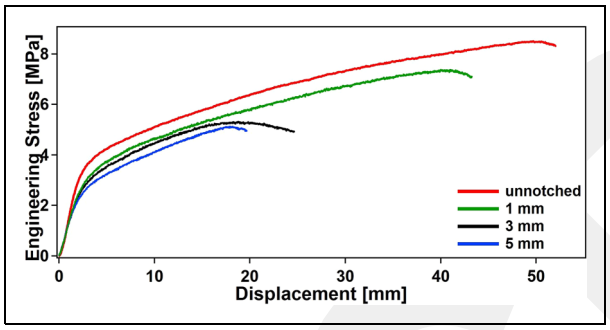

Figure 7. Engineering stress versus displacement response of unnotched and notched specimens with 1, 3, and 5 mm initial lengths.

SEM images observed from the different total displacements reveal that transition of the material behavior at yield stress and ultimate stress is substantially dependent on the fiber deformation mechanisms and also the interaction of the fibers at these stress values. Specimens that are strained below the yield stress show a decrease in the average fiber radii and elastic strains independent of the loading direction. Figure 9(a) and (b) shows SEM images of the undeformed and elastically deformed specimens, respectively. Subsequent uniaxial stress accumulation on the fibers results in plastic deformation as shown in Figure 9(c) that is observed from the strained specimen after yield. In this stage, plastically elongated fibers turn into an entangled structure throughout the membrane and with the further displacement levels it is observed that the entangled fibers merge and align through the loading direction (Figure 9(d)). Lastly, cleavage surface images reveal a complete degradation of the fiber structure before rupture as shown in Figure 9(e) and (f).

Corresponding fiber deformation with a stress displacement response of a 3 mm notch specimen is shown in the Appendix. It is observed that a macroscopic yielding response is due to the plastic deformation of uniaxially loaded individual fibers. Such a shear yielding mechanism with a subsequent neck propagation is also reported in previous studies for polymer nanofibers.[67–69] Additionally, multiple necking regions arise on the nanofiber indicate that uniaxial stress concentrates at several regions during plastic deformation as shown in Figure 9(c). Basically, shear yielding in polymer structures can be defined as a localized change in the shape without any increase or decrease of the volume, which is mostly accompanied by strain softening or local

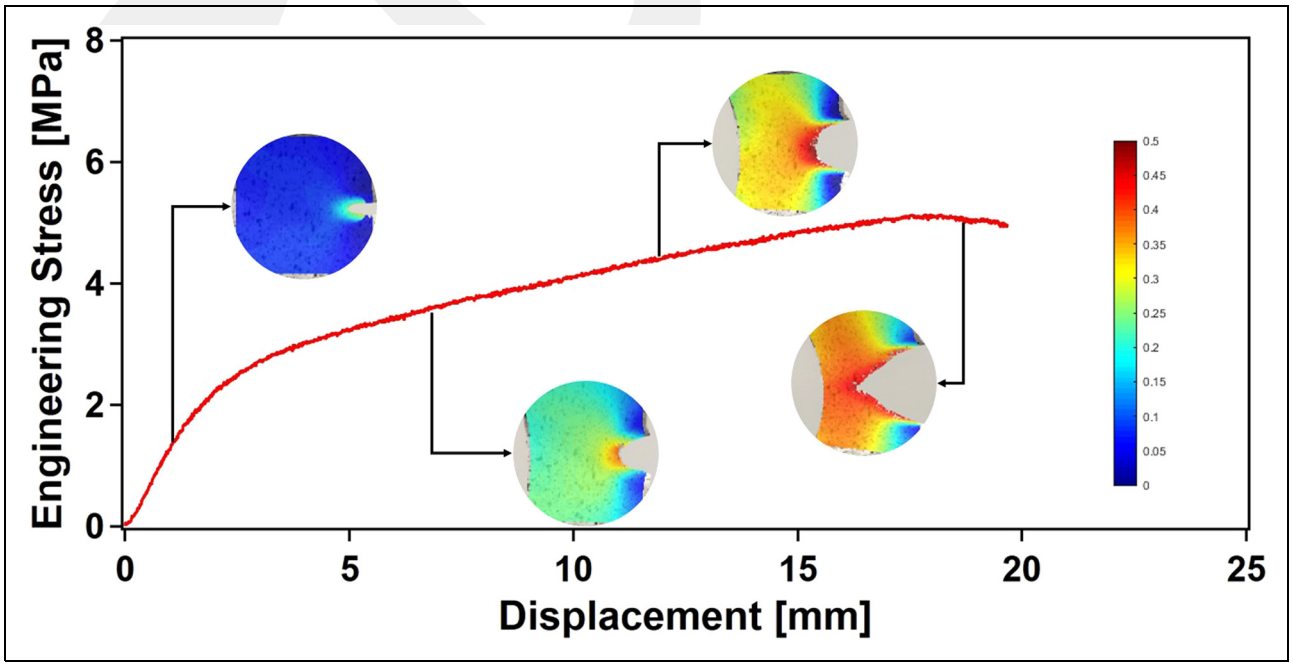

Figure 8. Eulerian strain distribution at the elastic region prior to yield and plastic regions after yield, prior to necking and after necking.

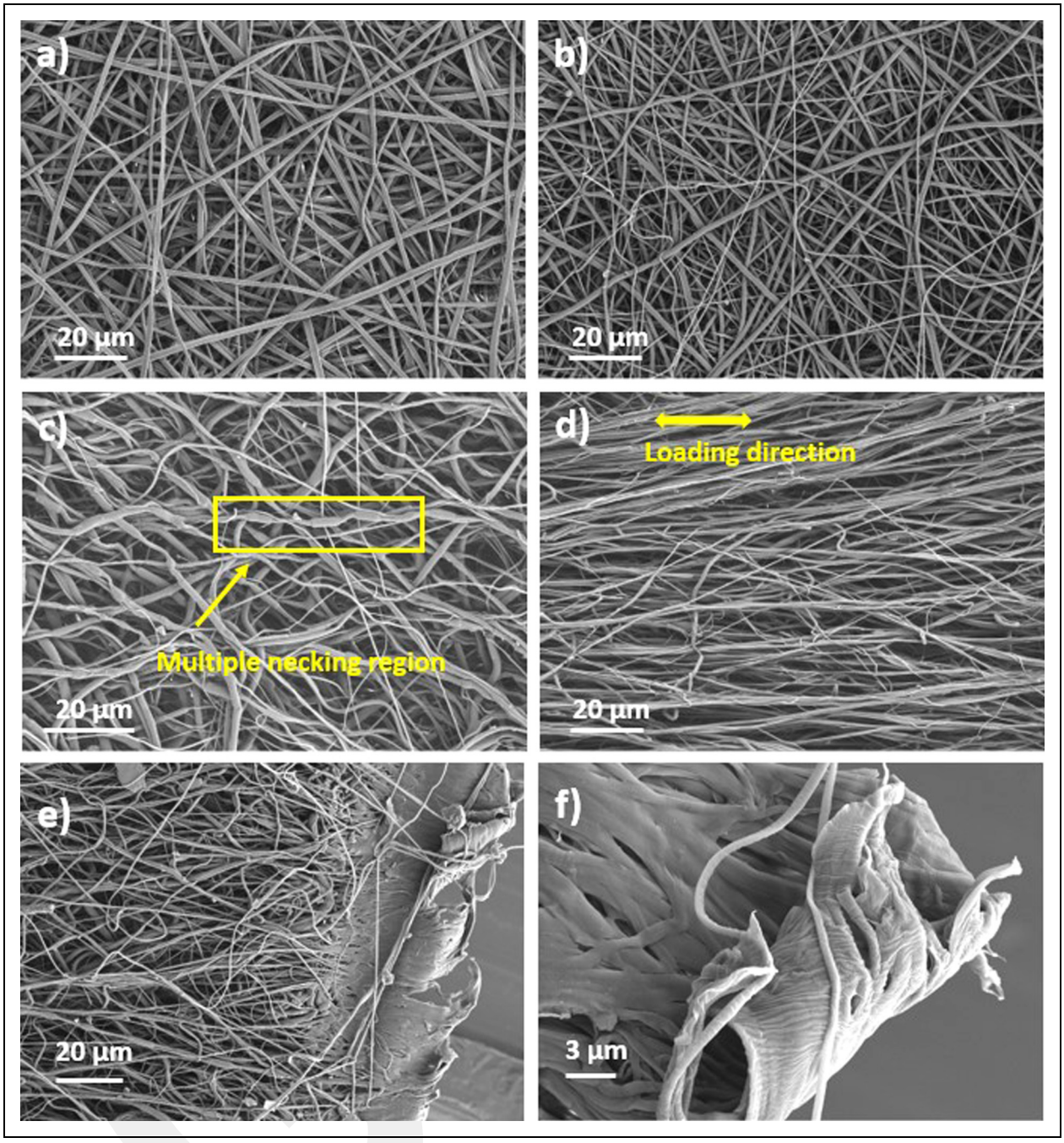

Figure 9. Scanning electron microscopy (SEM) images of the specimens in various total displacements: (a) undeformed, (b) prior to yield, (c) after yield, (d) prior to necking, and (e), (f) after necking.

geometric factors.[70] In further steps of plastic deformation, it is observed that most of the individual nanofibers merge by plastic elongation and a substantial decrease in the nanofiber diameter. Eventually, oriented and merged fibrous structures allow cleavage to propagate through the membrane.

Since uniaxial tension on the individual fibers results in microscopic deformation, it is important to evaluate hydrostatic stress or volumetric stress that arises ahead of the crack tip, which can be defined as average stress of the uniaxial stresses in all three dimensions. Hydrostatic stress results depending on the distance to the initial notch are shown in Figure 10. It is observed that as the initial notch length increases there is also an increase in the hydrostatic stress near the crack tip, whereas it is equilibrated in the same values for all specimens as the distance increases. It is important to note that more stress accumulation on 3 and 5 mm initial notched specimens leads to earlier failure compared to a 1 mm specimen as also observed in overall displacement and engineering stress behavior (Figure 7). Thus, it can be concluded that hydrostatic stress enhances the microstructural deformation mechanisms which lead to a decrease in macroscopic strength and ductility of the PCL membrane.

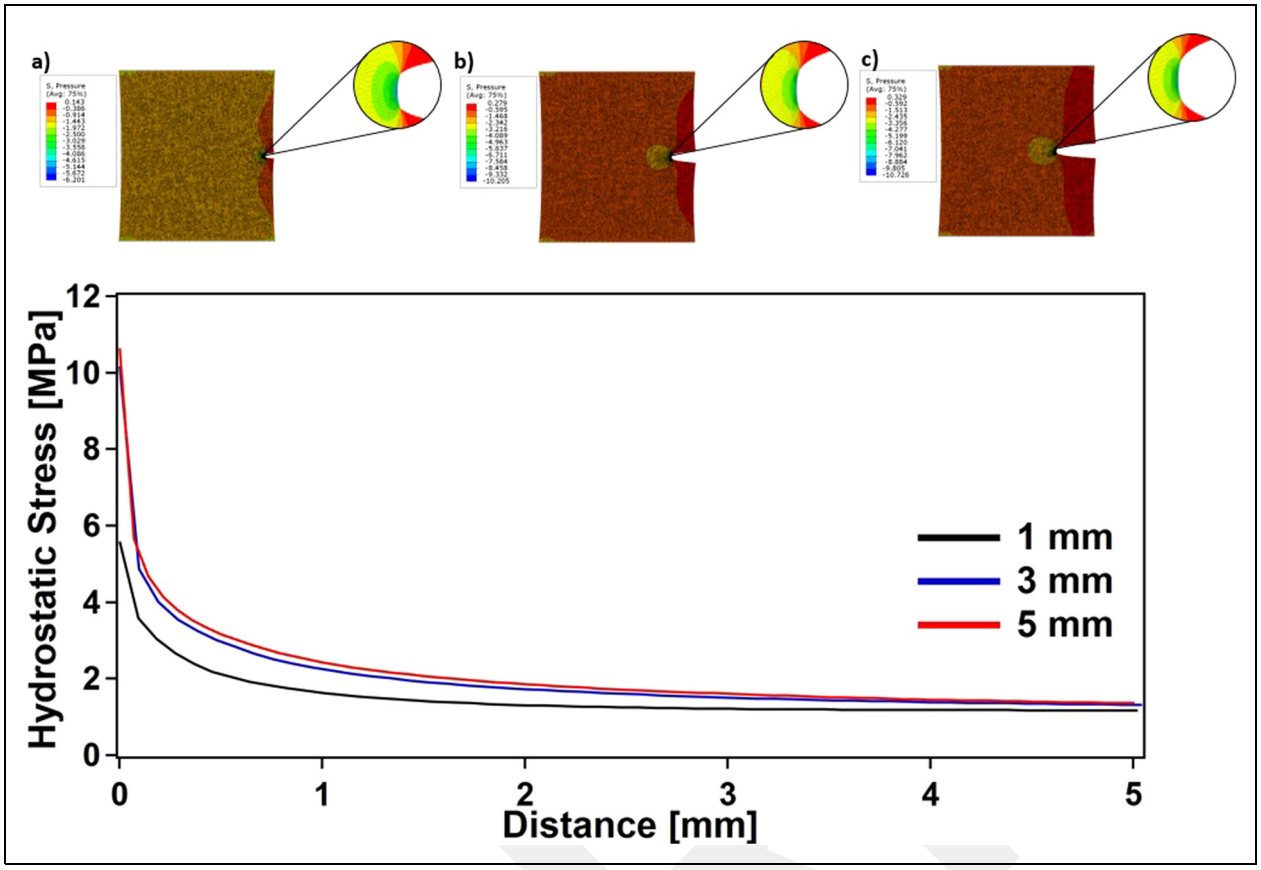

Figure 10. Hydrostatic stress distribution of the notched specimen prior to yield: (a) 1 mm, (b) 3 mm, and (c) 5 mm.

Conclusion

The current study comprehensively unveils the effects of strain rate, size, and pre-existing crack length on the mechanical properties of membranes for the first time in the literature. The strain rates, utilized to study the strain rate effect, were 10^{-1}, 10^{-2}, and 10^{-3} s^{-1}, respectively. Size effect tests were performed at the strain rate of 10^{-3} s^{-1}. Crack growth tests were conducted with initial pre-existing cracks of 1, 3, and 5 mm, respectively. From the study presented herein the following conclusions can be drawn:

1. Electrospun PCL membranes showed a positive strain rate sensitivity under tensile loading. The yield strength, UTS, and Young's modulus of electrospun PCL membranes increased as the strain rate increased from 10^{-3} to 10^{-1} s^{-1} sacrificing ductility.
2. The average fiber diameter decreases during the deformation. Thinner fibers result in less strength but more ductility.
3. The effects of the specimen geometry on the mechanical response of the PCL membranes have been demonstrated, and different applications were proposed for different sample dimensions.
4. Deformation and interaction of the individual nanofibers directly affected the macroscopic behavior. It is observed that higher stress concentration on local regions result in loss of fibrous properties and the porous structure of the electrospun membrane.
5. Notched specimen with 3 and 5 mm cause more hydrostatic stress concentration ahead of the crack tip compared with the 1 mm notch which enhances the propagation of the crack and results in earlier failure.

Declaration of conflicting interests

The authors declared no potential conflicts of interest with respect to the research, authorship, and/or publication of this article.

Funding

The authors received no financial support for the research, authorship, and/or publication of this article.

ORCID iD

Burak Bal https://orcid.org/0000-0002-7389-9155

Supplemental material

Supplemental material for this article is available online.

References

1. Politi S, Carotenuto F, Rinaldi A, et al. Smart ECM-based electrospun biomaterials for skeletal muscle regeneration. *Nanomaterials* 2020; 10: 1781.

2. Dziemidowicz K, Sang Q, Wu J, et al. Electrospinning for healthcare: recent advancements. *J Mater Chem C Mater* 2021; 9: 939–951.
3. Rahmani Del Bakhshayesh A, Mostafavi E, Alizadeh E, et al. Fabrication of three-dimensional scaffolds based on nano-biomimetic collagen hybrid constructs for skin tissue engineering. *ACS Omega* 2018; 3: 8605–8611.
4. Ye K, Kuang H, You Z, et al. Electrospun nanofibers for tissue engineering with drug loading and release. *Pharmaceutics* 2019; 11: 182.
5. Nikolova MP and Chavali MS. Recent advances in biomaterials for 3D scaffolds: a review. *Bioact Mater* 2019; 4: 271–292.
6. Wolf MT, Dearth CL, Sonnenberg SB, et al. Naturally derived and synthetic scaffolds for skeletal muscle reconstruction. *Adv Drug Deliv Rev* 2015; 84: 208–221.
7. Aksit NN, Gurdap S, Isoglu SD, et al. Preparation of antibacterial electrospun poly(D,L-lactide-co-glycolide)/gelatin blend membranes containing Hypericum capitatum var. capitatum. *Int J Polym Mater Polym Biomater* 2020; 70(11): 797–809.
8. Xie X, Chen Y, Wang X, et al. Electrospinning nanofiber scaffolds for soft and hard tissue regeneration *J. Mater Sci Technol* 2020; 59: 243–261.
9. Semitela Â, Girão AF, Fernandes C, et al. Electrospinning of bioactive polycaprolactone-gelatin nanofibres with increased pore size for cartilage tissue engineering applications. *J Biomater Appl* 2020; 35: 471–484.
10. Sharpe JM, Lee H, Hall AR, et al. Mechanical properties of electrospun, blended fibrinogen: PCL nanofibers. *Nanomaterials* 2020; 10: 1843.
11. Mohandesnezhad S, Pilehvar-Soltanahmadi Y, Alizadeh E, et al. In vitro evaluation of zeolite-nHA blended PCL/PLA nanofibers for dental tissue engineering. *Mater Chem Phys* 2020; 252: 123152.
12. Heidari M, Bahrami SH, Ranjbar-Mohammadi M, et al. Smart electrospun nanofibers containing PCL/gelatin/graphene oxide for application in nerve tissue engineering. *Mater Sci Eng C* 2019; 103: 109768.
13. Pişkin E, Işoğlu IA. Bölgen N, et al. In vivo performance of simvastatin-loaded electrospun spiral-wound polycaprolactone scaffolds in reconstruction of cranial bone defects in the rat model. *J Biomed Mater Res A* 2009; 90: 1137–1151.
14. Asti A and Gioglio L. Natural and synthetic biodegradable polymers: different scaffolds for cell expansion and tissue formation. *Int J Artif Organs* 2015; 37: 197–205.
15. Croisier F, Duwez AS, Jérôme C, et al. Mechanical testing of electrospun PCL fibers. *Acta Biomater* 2012; 8: 218–224.
16. Chen W, Xu Y, Liu Y, et al. Three-dimensional printed electrospun fiber-based scaffold for cartilage regeneration. *Mater Des* 2019; 179: 107886.
17. Unal S, Arslan S, Yilmaz BK, et al. Polycaprolactone/gelatin/hyaluronic acid electrospun scaffolds to mimic glioblastoma extracellular matrix. *Mater* 2020; 13: 2661.
18. Feng C, Chen Y, Shao J, et al. The crystallization behavior of poly(L-lactic acid)/poly(D-lactic acid) electrospun fibers: effect of distance of isomeric polymers *Ind Eng Chem Res* 2020; 59: 8480–8491.
19. Wulf K, Arbeiter D, Matschegewski C, et al. Smart releasing electrospun nanofibers—poly: l.lactide fibers as dual drug delivery system for biomedical application *Biomed Mater* 2021; 16: 015022.
20. Pitarresi G, Martorana A, Palumbo FS, et al. New gellan gum-graft-poly(D,L-lactide-co-glycolide) copolymers aspromising bioinks: synthesis and characterization. *Int J Biol Macromol* 2020; 162: 1653–1667.
21. Gámez E, Elizondo-Castillo H, Tascon J, et al. Antibacterial effect of thymol loaded SBA-15 nanorods incorporated in PCL electrospun fibers. *Nanomaterials* 2020; 10: 616.
22. Dwivedi R, Kumar S, Pandey R, et al. Polycaprolactone as biomaterial for bone scaffolds: review of literature. *J Oral Biol Craniofac Res* 2020; 10: 381–388.
23. Wang L and Xin B. Poly(L-lactide-co-ϵ-caprolactone) nanofiber morphology control and influence of properties. *J Phys Conf Ser* 2021; 1790: 012062.
24. Mondragón M, López-Villegas O, Sánchez-Valdés S, et al. Effect of thermoplastic starch and photocrosslinking on the properties and morphology of electrospun poly(ethylene-co-vinyl alcohol) mats. *Poly Eng Sci* 2020; 60: 474–480.
25. Mondal D, Griffith M and Venkatraman SS. Polycaprolactone-based biomaterials for tissue engineering and drug delivery: current scenario and challenges. *Int J Poly Mater Poly Biomater* 2016; 65: 255–265.
26. Song R, Murphy M, Li C, et al. Current development of biodegradable polymeric materials for biomedical applications. *Drug Des Dev Ther* 2018; 12: 3117–3145.
27. Maccaferri E, Mazzocchetti L, Benelli T, et al. Rubbery nanofibers by co-electrospinning of almost immiscible NBR and PCL blends. *Mater Des* 2020; 186: 108210.
28. Abedalwafa M, Wang F, Wang L, et al. Biodegradable PCL for tissue engineering applications: a review. *Rev Adv Mater Sci* 2013; 34: 123–140.
29. Sabra S, Ragab D, Agwa MM, et al. Recent advances in electrospun nanofibers for some biomedical applications. *Eur J Pharm Sci* 2020; 144: 105224.
30. Gorrasi G, Longo R and Viscusi G. Fabrication and characterization of electrospun membranes based on "poly (ϵ-caprolactone)","poly (3-hydroxybutyrate)" and their blend for tunable drug delivery of curcumin. *Polymers* 2020; 12: 2239.
31. Alexeev D, Goedecke N, Snedeker J, et al. Mechanical evaluation of electrospun poly (ϵ-caprolactone) single fibers. *Mater Today Commun* 2020; 24: 101211.
32. Can-Herrera LA, Oliva AI, Dzul-Cervantes MAA, et al. Morphological and mechanical properties of electrospun polycaprolactone scaffolds: effect of applied voltage. *Polymers* 2021; 13: 662.
33. Dziadek M, Zagrajczuk B, Menaszek E, et al. Poly (ϵ-caprolactone)-based membranes with tunable physicochemical, bioactive and osteoinductive properties. *J Mater Sci* 2017; 52: 12960–12980.
34. Tan EP, Ng SY and Lim CT. Tensile testing of a single ultrafine polymeric fiber. *Biomaterials* 2005; 26: 1453–1456.
35. Ho MH, Do TBT, Dang NNT, et al. Effects of an acetic acid and acetone mixture on the characteristics and scaffold–cell interaction of electrospun polycaprolactone membranes. *Appl Sci* 2019; 9: 4350.
36. Bal B, Tugluca IB, Koc N, et al. On the detailed mechanical response investigation of PHBV/PCL and PHBV/PLGA electrospun mats. *Mater Res Express* 2019; 6: 065411.
37. Eqtesadi S, Motealleh A, Pajares A, et al. Influence of sintering temperature on the mechanical properties of ϵ-PCL-impregnated 45S5 bioglass-derived scaffolds fabricated by robocasting. *J Eur Ceram Soc* 2015; 35: 3985–3993.

38. Duling RR, Dupaix RB, Katsube N, et al. Mechanical characterization of electrospun polycaprolactone (PCL): a potential scaffold for tissue engineering. *J Biomech Eng* 2008; 130: 1–13.
39. Chou SF and Woodrow KA. Relationships between mechanical properties and drug release from electrospun fibers of PCL and PLGA blends. *J Mech Behav Biomed Mater* 2017; 65: 724–733.
40. Yin Y and Xiong J. Effect of the distribution of fiber orientation on the mechanical properties of silk fibroin/polycaprolactone nanofiber mats. *J Eng Fiber Fabr* 2017; 12: 17–28.
41. Wong SC, Baji A and Leng S. Effect of fiber diameter on tensile properties of electrospun poly(ϵ-caprolactone). *Polymers* 2008; 49: 4713–4722.
42. Drilling S, Gaumer J and Lannutti J. Fabrication of burst pressure competent vascular grafts via electrospinning: effects of microstructure. *J Biomed Mater Res A* 2009; 88: 923–934.
43. Drexler JW and Powell HM. Regulation of electrospun scaffold stiffness via coaxial core diameter. *Acta Biomater* 2011; 7: 1133–1139.
44. Baylan N, Bhat S, Ditto M, et al. Polycaprolactone nanofiber interspersed collagen type-I scaffold for bone regeneration: a unique injectable osteogenic scaffold. *Biomed Mater* 2013; 8: 045011.
45. Oliveira JE, Mattoso LHC, Orts WJ, et al. Structural and morphological characterization of micro and nanofibers produced by electrospinning and solution blow spinning: a comparative study. *Adv Mater Sci Eng* 2013; 2013: 1–14.
46. Coleman MM, Zarian J and Section PS. Fourier-transform infrared studies of polymer blends. II. Poly (ε-caprolactone)–poly (vinyl chloride) system. *J Polym Sci B Polym Phys* 1979; 17: 837–850.
47. He Y and Inoue Y. Novel FTIR method for determining the crystallinity of poly (e-caprolactone). *Polym Int* 2000; 626: 623–626
48. Amani H, Arzaghi H, Bayandori M, et al. Controlling cell behavior through the design of biomaterial surfaces: a focus on surface modification techniques. *Adv Mater Int* 2019; 6: 1900572.
49. Hadj-hamou AS and Yahiaoui F. Performances of PCL/PVC/organoclay nanobioblends films for packaging applications. *Macromol Symp* 2019; 386: 1800239.
50. Hinestroza HP, Urena-Saborio H, Zurita F, et al. Nanocellulose and polycaprolactone nanospun composite membranes and their potential for the removal of pollutants from water. *Molecules* 2020; 25: 683.
51. Kostakova EK, Meszaros L, Maskova G, et al. Crystallinity of electrospun and centrifugal spun polycaprolactone fibers: a comparative study. *J Nanomater* 2017; 2017: 1–9.
52. Hussein M. Effects of strain rate and temperature on the mechanical behavior of carbon black reinforced elastomers based on butyl rubber and high molecular weight polyethylene. *Results Phys* 2018; 9: 511–517.
53. Amjadi M and Fatemi A. Tensile behavior of high-density polyethylene including the effects of processing technique, thickness, temperature, and strain rate. *Polymers* 2020; 12: 1857.
54. Wang W, Ma Y, Yang M, et al. Strain rate effect on tensile behavior for a high specific strength steel : from quasi-static to intermediate strain rates. *Metals* 2018; 8: 11.
55. Cao Y, Ahlström J and Karlsson B. The influence of temperatures and strain rates on the mechanical behavior of dual phase steel in different conditions. *J Mater Res Technol* 2015; 4: 68–74.
56. Zinszner JL, Erzar B and Forquin P. Strain rate sensitivity of the tensile strength of two silicon carbides: experimental evidence and micromechanical modelling. *Philos Trans A Math Phys Eng Sci* 2017; 375: 20160167.
57. Li S, Kang Y, Zhu G, et al. Effects of strain rates on mechanical properties and fracture mechanism of DP780 dual phase steel. *J Mater Eng Perform* 2015; 24: 2426–2434.
58. Szyniszewski S, Vogel R, Bittner F, et al. Non-cuttable material created through local resonance and strain rate effects. *Sci Rep* 2020; 10: 1–24.
59. Chen W, Hao H, Jong M, et al. Quasi-static and dynamic tensile properties of basalt fibre reinforced polymer. *Compos B Eng* 2017; 125: 123–133.
60. Bal B, Gumus B and Canadinc D. Incorporation of dynamic strain aging into a viscoplastic self-consistent model for predicting the negative strain rate sensitivity of hadfield steel. *J Mater Eng Technol* 2017; 138: 1–8.
61. Bal B, Koyama M, Canadinc D, et al. On the utility of crystal plasticity modeling to uncover the individual roles of microdeformation mechanisms on the work hardening response of Fe-23Mn-0.5C TWIP steel in the presence of hydrogen. *Trans ASME J Mater Eng Technol* 2018; 140: 1–13.
62. Alberola N, Fugier M, Petit D, et al. Tensile mechanical behaviour of quenched and annealed isotactic polypropylene films over a wide range of strain rates – part II relationship with microstructure. *J Mater Sci* 1995; 30: 860–868.
63. Shan GF, Yang W, Yang MB, et al. Investigation on tensile deformation behavior of semi-crystalline polymers. *J Macromol Sci B Phys* 2009; 48: 799–811.
64. Setton LA, Elliott DM and Mow VC. Altered mechanics of cartilage with osteoarthritis: human osteoarthritis and an experimental model of joint degeneration. *Osteoarthr Cartil* 1999; 7: 2–14.
65. Zhang Q, Du Q, Zhao Y, et al. Graphene oxide-modified electrospun polyvinyl alcohol nanofibrous scaffolds with potential as skin wound dressings. *RSC Adv* 2017; 7: 28826–28836.
66. Stachewicz U, Peker I, Tu W, et al. Stress delocalization in crack tolerant electrospun nanofiber networks. *ACS Appl Mater Interfaces* 2011; 3: 1991–1996.
67. Kim GM, Lach R, Michler GH, et al. Relationships between phase morphology and deformation mechanisms in polymer nanocomposite nanofibres prepared by an electrospinning process. *Nanotechnol* 2006; 17: 963–972.
68. Naraghi M, Kolluru PV and Chasiotis I. Time and strain rate dependent mechanical behavior of individual polymeric nanofibers. *J Mech Phys Solids* 2014; 62: 257–275.
69. Zussman E, Rittel D and Yarin AL. Failure modes of electrospun nanofibers. *Appl Phys Lett* 2003; 82: 3958–3960.
70. Kinloch AJ and Young RJ. *Shear yielding in fracture behaviour polymers*. Netherlands: Springer, 1995, pp. 107–146.

Appendix

The FTIR spectrum of the electrospun PCL membrane is shown in Supplemental Figure 11. Cell viability results are given in Supplemental Figure 12. XRD analysis of the PCL membrane is given in Supplemental Figure 13. Fiber

deformation with a stress displacement response of a 3 mm notch specimen is shown in Supplemental Figure 14.

Notation

kV	electrical voltage (V)
ml/h	flow rate of polymer solution
w/v	concentration of polymer solution

Greek symbol

μ	micron

Abbreviation

DIC	digital image correlation
DMEM	Dulbecco's modified Eagle medium
FBS	fetal bovine serum
FTIR	Fourier transform infrared spectroscopy
HFIP	hexafluoro-2-propanol
PCL	polycaprolactone
SEM	scanning electron microscopy
UTS	ultimate tensile strength
XRD	x-ray diffraction